JOURNAL OF MOLECULAR SPECTROSCOPY 72, 463–483 (1978)

Far Infrared Laser Magnetic Resonance Spectrum of CH

J. T. HOUGEN

National Bureau of Standards, Washington, D. C. 20234

J. A. MUCHA,[1] D. A. JENNINGS, AND K. M. EVENSON

National Bureau of Standards, Boulder, Colorado 80302

Laser magnetic resonance spectra between 0 and 17 kG have been recorded and analyzed for $(J' \leftarrow J'') = (\frac{3}{2} \leftarrow \frac{1}{2})$, $(\frac{1}{2} \leftarrow \frac{1}{2})$, and $(\frac{1}{2} \leftarrow \frac{3}{2})$ transitions in the CH molecule, using the optically pumped far infrared lasers: 118.8 μm (CH_3OH), 180.7 μm (CD_3OH), 554.4 μm (CH_2CF_2), 561.3 μm (DCOOD), and 567.9 μm (CH_2CHCl). Other transitions in CH were detected with the $^{13}CH_3OH$ laser at 115.8, 149.3, and 203.6 μm. The CH radical was generated in a low-pressure methane and atomic fluorine flame within the laser cavity. Analysis of the $M'_J \leftarrow M''_J$ structure yields wavenumbers for the rotational transitions mentioned above of 84.3494, 55.3397, and 17.8376 cm^{-1}, respectively. Combining results from the M_J analysis with the $J = \frac{1}{2}$ Λ-doubling interval derived from radioastronomy measurements yields Λ-doubling values for the $J = \frac{3}{2}$, $\frac{5}{2}$, and $\frac{7}{2}$ states of 0.0237, 0.1620, and 0.3759 cm^{-1}, respectively. Both the rotational intervals and the Λ-doublings are in good agreement with earlier less precise optical results. Analysis of the hyperfine structure yields values for the Frosch and Foley hyperfine parameters of $a = +52$, $b = -74$, $c = +52$, and $d = +43.6$ MHz, in good agreement with recent *ab initio* estimates and radioastronomy measurements.

I. INTRODUCTION

The electronic spectrum of CH has been studied extensively (*1*) and vibration–rotation levels of many electronic states are known with an accuracy of 0.01 to 0.1 cm^{-1}. In particular, the low-lying rotational levels of the $X^2\Pi_r$ ground state of CH have been well characterized by Douglas and Elliott (*2*). Higher precision studies of vibration–rotation or pure rotation spectra within the electronic ground state have not been successful with conventional infrared or microwave laboratory techniques; the only studies of such transitions previously reported consist of the laser magnetic resonance observation (*3*) near 84 cm^{-1} of a $v = 0$, $J' = \frac{1}{2} \leftarrow J'' = \frac{3}{2}$ transition (primes and double primes indicate upper and lower state quantities, respectively), and the radioastronomical observations (*4*) near 3.3 GHz of the Λ-doubling transition for $v = 0$ and $J = \frac{1}{2}$.

In the present work, which extends the earlier laser magnetic resonance study (*3*), we present analyses of spectra recorded with five additional far infrared laser lines.

[1] NBS–NRC Postdoctoral Research Associate, 1975–77. Present address: Bell Laboratories, Murray Hill, NJ 07974.

0022-2852/78/0723-0463$02.00/0
Copyright © 1978 by Academic Press, Inc.
All rights of reproduction in any form reserved.

These five spectra involve only two additional CH rotational transitions, but it proved necessary for complete analysis to record some transitions with more than one laser line. A recently discovered new set of laser lines from $^{13}CH_3OH$ (*5*) has just provided three additional spectra assigned to three other rotational transitions; however, complete analysis of these observations must await refined data. Figure 1 illustrates the rotational transitions of CH observed in laser magnetic resonance studies. Table I summarizes related experimental information. Rotational energy differences obtained from the spectra analyzed here are significantly better determined than corresponding differences obtained from the electronic spectrum (*2*).

Rotational wavefunctions and energy levels of $^2\Pi$ states can be labeled using either Hund's case (*a*) notation or Hund's case (*b*) notation (*9*). In this paper we shall, on the one hand, use case (*a*) notation to label the rotational *basis set* functions used in carrying out the theoretical calculations, since this greatly simplifies setting up the Hamiltonian matrices. In case (*a*), rotational functions with $J > \frac{1}{2}$ are assigned to either the $^2\Pi_{\frac{3}{2}}$ or $^2\Pi_{\frac{1}{2}}$ spin component of the nonrotating molecule. We shall, on the other hand, use case (*b*) notation to label rotational wavefunctions and energy levels obtained by diagonalizing the Hamiltonian matrices, i.e., to label wavefunctions and energy levels actually belonging to the CH molecule, as in Fig. 1 and Table I, since case (*a*) notation is singularly inappropriate for the $X^2\Pi$ state of CH with $A \cong 2B$. (When $A = 2B$, all molecular rotational wavefunctions with $J > \frac{1}{2}$ are an exactly equal mixture of case (*a*) $^2\Pi_{\frac{3}{2}}$ and $^2\Pi_{\frac{1}{2}}$ basis set functions for that J, whereas these same molecular wavefunctions are very nearly equal to one or the other of the case (*b*) basis set functions.) In case (*b*), rotational levels are characterized by a quantum number N, where $N = J \mp \frac{1}{2}$ for $F_1(N)$ and $F_2(N)$ levels, respectively. The level with $N = J - \frac{1}{2}$ always lies lower in energy than the level with $N = J + \frac{1}{2}$, *for the same* J.

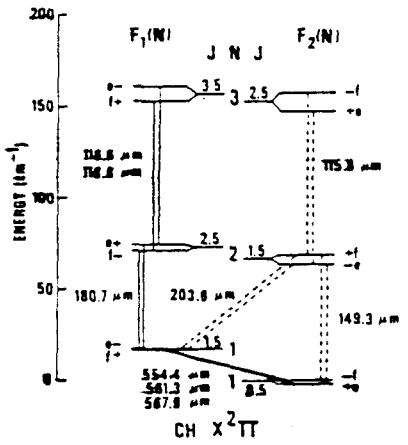

FIG. 1. Energy level diagram for the low-lying rotational states of the $X^2\Pi$ state of CH (*2*). Rotational levels are drawn to scale in the center of the diagram and labeled by the rotational quantum numbers N and J. Λ-doublings are magnified 20-fold and shown at the edges of the diagram; the resultant levels are labeled by their parities. Wavelengths of the far infrared laser lines used to obtain magnetic resonance spectra of the indicated transitions are given in the figure. Spectra observed with the 115.8, 149.3, and 203.6 μm lines (indicated by the dashed transitions) have not been analyzed in the present work.

TABLE I

Rotational Transitions of CH Observed in Laser Magnetic Resonance Studies

Laser Characteristics				CH Rotational Transitions		
Pump[a]	Gain Medium	λ [μm]	ν [cm^{-1}]	(N',J')–(N",J")	(g_J')[b]	(g_J")[b]
10 R(16)	$^{13}CH_3OH$	115.8	86.33845[c]	(3,5/2)-(2,3/2)[g]	+0.152	+0.062
Discharge	H_2O	118.6	84.32340[d]	(3,7/2)-(2,5/2)[h]	-0.341	-0.495
9 P(36)	CH_3OH	118.8	84.15092[e]	(3,7/2)-(2,5/2)[i]	-0.341	-0.495
9 P(22)	$^{13}CH_3OH$	149.3	66.99168[c]	(2,3/2)-(1,1/2)[g]	+0.062	+0.001
10 R(34)	CD_3OH	180.7	55.32794[c]	(2,5/2)-(1,3/2)[i]	-0.495	-0.863
10 R(16)	$^{13}CH_3OH$	203.6	49.10728[c]	(2,3/2)-(1,3/2)[g]	+0.062	-0.863
10 P(14)	CH_2CF_2	554.4	18.03865[e]	(1,3/2)-(1,1/2)[i]	-0.863	+0.001
10 P(20)	DCOOD	561.3	17.81598[f]	(1,3/2)-(1,1/2)[i]	-0.863	+0.001
10 P(16)	CH_2CHCl	567.9	17.60731[e]	(1,3/2)-(1,1/2)[i]	-0.863	+0.001

[a] The gain medium was pumped by electric discharge or by a CO_2 laser line of the 9 μm or 10 μm band.

[b] Magnetic g-values, calculated from Eqs. (11) and valid for a $^2\Pi$ state with A = 28 when H ≈ 0.

[c] From the precise frequency measurements of (5).

[d] From the precise frequency measurements of (6).

[e] From the precise frequency measurements of (7).

[f] From the precise frequency measurements of (8).

[g] Spectrum recorded and tentatively assigned, but not completely analyzed.

[h] Spectrum recorded and assigned in (3).

[i] Spectrum recorded and analyzed in the present paper.

We adopt as parity labels the subscripts *e* and *f* (*10*), which indicate that the rotational state in question has parity $+(-1)^{J-\frac{1}{2}}$ or $-(-1)^{J-\frac{1}{2}}$, respectively.

The rest of this paper is divided into sections containing experimental details (II), the theoretical model (III), details of the least squares fits of the M_J structure (IV) and the hyperfine structure (V), and some discussion of the results (VI).

II. EXPERIMENTAL METHOD

Spectra were obtained with a newly constructed CO_2-transversely-pumped far-infrared magnetic resonance spectrometer (*11*), shown in Fig. 2. Precise values of the far infrared laser wavenumbers used in this work, together with the mode of excitation are given in Table I. The far infrared laser radiation remained stable to within 0.00003 cm^{-1} of the values in the table during measurement.

The magnetic field could be scanned from 0 to 20 kG (10 kG = 1 T), though accurate field measurements were possible only below 17 kG. For these accurate measurements, magnetic fields were recorded with a precision of ±0.1 G using a nuclear magnetic

OPTICALLY PUMPED LASER MAGNETIC RESONANCE SPECTROMETER

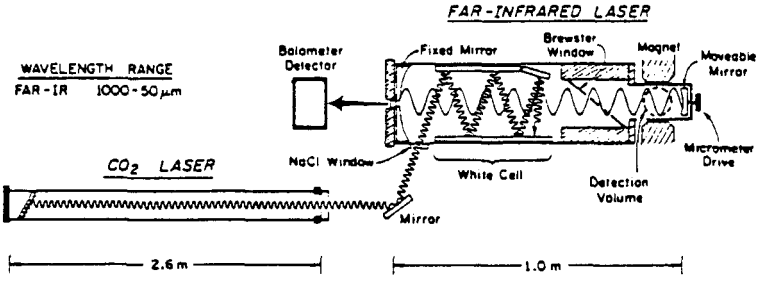

FIG. 2. The laser magnetic resonance spectrometer used in this work.

resonance digital Gaussmeter. Corrections to the Gaussmeter field measurements for instrument calibration and geometrical effects range from 1 to 60 G over the 0 to 17 kG scan. It is believed that the corrected field values have an accuracy near ±1 G.

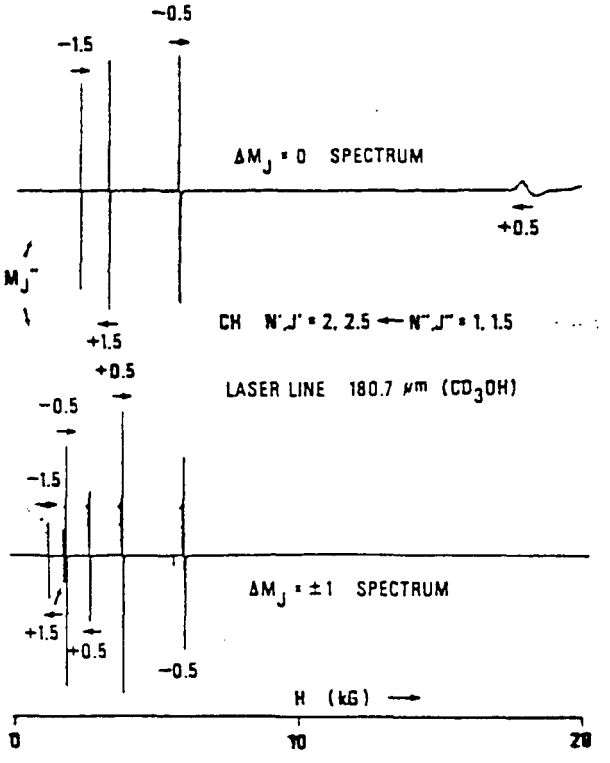

FIG. 3. A magnetic resonance survey spectrum of CH from 0 to 20 kG, recorded with the 180.7 μm line of CD_3OH. The upper and lower traces correspond to parallel and perpendicular polarization, respectively, of the electric field vector of the laser radiation with respect to the external magnetic field. Lines marked above or below with a horizontal arrow were shown experimentally to shift in the indicated direction when the laser is pulled to slightly higher frequency. The lower state quantum number M_J'' is given above each line belonging to the $F_{1f}(2) \leftarrow F_{1f}(1)$ transition and below each line belonging to the $F_{1e}(2) \leftarrow F_{1e}(1)$ transition of CH shown in Fig. 1.

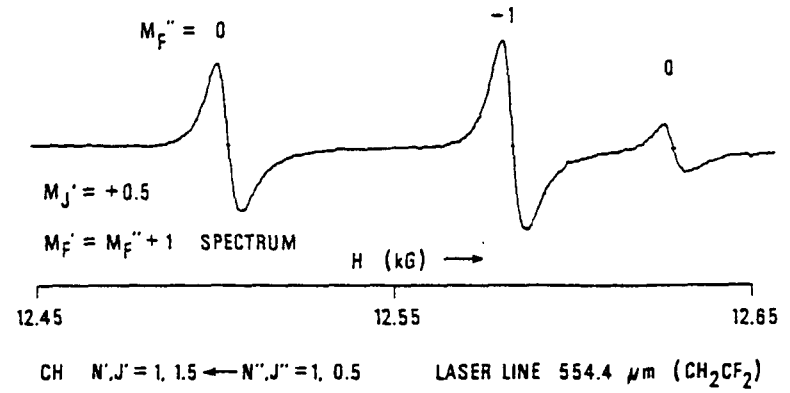

FIG. 4. The hyperfine pattern of a $v = 0$ $F_{1f}(1) \leftarrow F_{2f}(1)$ transition, recorded in perpendicular polarization with the 554.4 μm line of CH_2CF_2, under conditions such that the linewidths (in MHz) are determined by pressure and Doppler broadening. A three-line hyperfine pattern is observed because the $J'' = \frac{1}{2}$ state has an extremely small g_J value and the high-field coupling limit (with good quantum numbers M_I and M_J) applies only to the $J' = \frac{1}{2}$ state. The lower state quantum number $M_F'' = M_I'' + M_J''$ is shown for each line. The combined intensity of the two $M_F'' = 0$ lines is approximately equal to the intensity of the $M_F'' = -1$ line.

Since the Bohr magneton μ_B has a value of 1.4 MHz/G, and since the M_J components of rotational levels vary in energy as $-g_J\mu_B M_J H$, where approximate g_J values for CH are given in Table I, the accuracy of the magnetic field measurements would seem to permit energy level determinations to ±1 MHz. Attaining such accuracy in practice is quite difficult. Qualitatively speaking, the difficulty arises from the fact that absorption resonances observed near 10 kG involve magnetic shifts of the energy levels approx-

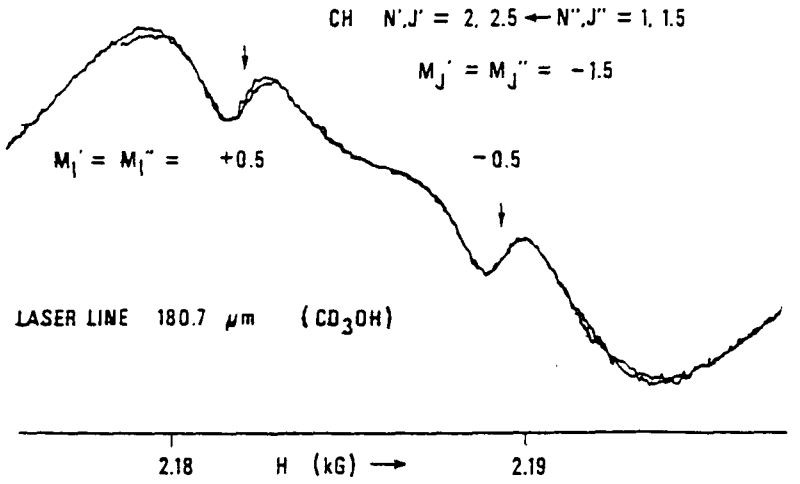

FIG. 5. Lamb-dip measurement of the hyperfine splitting in the first line of the parallel-polarization spectrum shown in Fig. 3. Chopping and detection electronics are such that a Doppler-broadened line-derivative profile first rises and then falls as H increases, while the associated Lamb-dips fall and then rise. This two-line pattern corresponds to the high-field coupling limit. Upper and lower state quantum numbers are shown for each Lamb dip.

imating 10 000 MHz. One must thus extrapolate the Zeeman levels back to 0 kG with an accuracy of 1 part in 10^4 to achieve the desired ± 1 MHz uncertainties. In the present work we were able to achieve, with some difficulty, uncertainties of ± 6 MHz.

In the earlier measurements CH radicals were generated in an oxygen–acetylene flame (*3*) at higher pressures and from C_3O_2 and H atoms for the lower pressure hyperfine measurements. In the present work, CH was generated by reacting CH_4 with F atoms (formed in a microwave-discharged mixture of F_2 in He) under flow conditions achieved

TABLE II

Magnetic Field Values,[a] Assignments,[b] and Observed-minus-Calculated[c] Values for the $J' = \frac{1}{2} \leftarrow J'' = \frac{1}{2}$ Transitions of CH

				Spectra recorded with the 567.9 μm line of CH_2CHCl								Spectra with 561.3 μm of DCOOD			
				$F_{1e}(1) - F_{2e}(1)$		$F_{1e}(1) - F_{2e}(1)$		$F_{1f}(1) - F_{2f}(1)$		$F_{1f}(1) - F_{2f}(1)$		$F_{1e}(1) - F_{2e}(1)$		$F_{1e}(1) - F_{2e}(1)$	
Assignment				v = 0		v = 1		v = 0		v = 1		v = 0		v = 1	
M_I'	M_J'	M_I''	M_J''	H [kG]	O-C [G]	H [kG]	O-C [G]	H [kG]	O-C [G]	H [kG]	O-C [G]	H [kG]	O-C [G]	H [kG]	O-C [G]
-1/2	-1/2	+1/2	-1/2	15.9646	-0.2	13.0738	-0.0	8.3213	+0.1	5.9950	-0.9	4.5040	-0.5	1.7969	-0.4
+1/2	-1/2		(-)	15.9802	+0.2	13.0938	-0.0	8.4247	+0.2	6.1012	+0.2	4.5248	-0.1	1.8235	-0.4
+1/2	-1/2		(+)	-	-	-	-	8.2896	+0.2	5.9750	-0.3	4.4439	+0.4	-	-
+1/2	-1/2	+1/2	+1/2	15.7575	-0.6	12.9251	+0.0	8.3313	-0.4	6.0049	-0.2	(4.4662)	+1.3	(1.7883)	-0.1
-1/2	-1/2		(+)	15.7690	+0.6	12.9335	+0.0	8.3553	-0.1	6.0215	+0.8	(4.4662)	-1.1	(1.7883)	+0.9
-1/2	-1/2		(-)	-	-	-	-	8.4917	-0.1	6.1480	+0.5	-	-	-	-
-1/2	-3/2	-1/2	-1/2	4.9300	+0.4	4.0933	+0.2	2.6763	+0.2	(1.9466)	-0.2	1.4647	+0.4	0.5902	-0.6
+1/2	-3/2		(-)	4.9424	-0.2	4.1075	-0.2	2.7126	-0.0	1.9851	+0.2	1.4781	-0.4	0.6082	+0.6
+1/2	-3/2		(+)	4.9136	-0.2	-	-	2.6729	-0.2	(1.9466)	+0.0	-	-	-	-
	-1/2		-1/2	15.9722	-1.2	13.0834	-1.9	8.3508	-0.1	6.0260	-0.2	4.5139	-0.0	1.8083	-0.3
	-1/2		+1/2	15.7635	+1.4	12.9297	+3.2	8.3657	+0.3	6.0355	+0.4	4.4669	+0.0	1.7902	-0.3
	-3/2		-1/2	4.9359	-0.5	4.1000	+2.4	2.6856	-0.6	1.9572	-0.5	1.4707	+0.1	0.5978	+1.6

				Spectra with 561.3 μm of DCOOD				Spectra recorded with the 554.4 μm line of CH_2CF_2							
				$F_{1f}(1) - F_{2f}(1)$		$F_{1f}(1) - F_{2f}(1)$		$F_{1e}(1) - F_{2e}(1)$		$F_{1e}(1) - F_{2e}(1)$		$F_{1f}(1) - F_{2f}(1)$		$F_{1f}(1) - F_{2f}(1)$	
Assignment				v = 0		v = 1		v = 0		v = 1		v = 0		v = 1	
M_I'	M_J'	M_I''	M_J''	H [kG]	O-C [G]	H [kG]	O-C [G]	H [kG]	O-C [G]	H [kG]	O-C [G]	H [kG]	O-C [G]	H [kG]	O-C [G]
+1/2	+1/2	+1/2	+1/2	2.2579	-0.9	obscured	-	6.4887	+0.0	9.0808	+0.0	12.5734	-0.1	14.7608	-0.1
-1/2	+1/2		(+)	2.2531	-0.3	4.4870	+0.6	6.4681	+0.4	9.0576	+0.2	12.5464	+0.1	14.7289	+0.2
-1/2	+1/2		(-)	2.1377	-0.1	4.3738	-0.5	6.3629	-0.4	-	-	12.4227	-0.2	14.5996	+0.4
-1/2	+1/2	-1/2	-1/2	2.2632	+0.3	4.5027	-1.2	(6.4151)	+0.0	(8.9831)	-0.1	12.5831	+0.1	14.7660	-0.1
+1/2	+1/2		(-)	2.1525	+0.1	4.4083	+1.1	(6.4151)	-0.1	(8.9831)	-0.1	12.5040	+0.1	14.6967	-0.3
+1/2	+1/2		(+)	2.2697	+0.8	-	-	-	-	-	-	12.6284	-0.0	14.8276	-0.1
+1/2	+3/2	+1/2	+1/2	(0.7609)	+0.0	1.5274	-	2.2168	-0.4	3.1345	+0.2	4.4114	+0.1	5.2220	-0.5
-1/2	+3/2		(+)	(0.7609)	+0.0	-	-	2.2054	+0.2	3.1210	-0.1	4.4080	-0.4	5.2170	+0.4
-1/2	+3/2		(-)	0.7216	-0.1	-	-	2.1917	+0.2	3.1017	-0.1	4.3691	+0.3	5.1777	+0.1
	+1/2		+1/2	2.2298	-0.1	4.4711	+0.3	6.4776	-0.1	9.0686	-0.6	12.5449	-0.9	14.7327	-2.9
	+1/2		-1/2	2.2341	-0.1	4.4778	+0.5	6.4157	+0.1	8.9837	+1.2	12.5585	+0.5	14.7437	+4.0
	+3/2		+1/2	0.7514	+0.7	1.5171	-2.2	2.2107	+0.0	3.1272	-1.6	4.4018	+1.1	5.2122	-2.9

[a] The first 9 rows of numbers in each column headed H represent actual field measurements of laser magnetic resonance lines (3 with $\Delta M_F = 0$, 6 with $\Delta M_F = \pm 1$), listed in order of decreasing intensity within each group of three; missing entries indicate lines too weak to observe; measurements in parentheses have two assignments. The last 3 rows of numbers in each column headed H represent hypothetical magnetic field values for transitions free of proton hyperfine effects, as obtained from Eq. (31).

[b] For actual magnetic field measurements, assignments are given for the upper state quantum numbers M_I' and M_J'; the lower state quantum numbers M_I'' and M_J'' are also given when $M_F'' = \pm 1$; only a sign is given when $M_F'' = 0$, indicating the appropriate sign choice in Eq. (27). For hypothetical hyperfine-free field values, only upper and lower state M_J assignments are given.

[c] The first 9 entries in each column headed O-C are obtained from one of four least squares hyperfine fits using Eq. (29); measurements of all lines belonging to a given rotational transition, i.e. measurements recorded with all three laser lines, were combined in a single fit. The last 3 entries in each column headed O-C are obtained from individual three-line M_J fits to Eq. (18).

with an 18 *l*/sec mechanical forepump. Approximate partial pressures of CH_4, F_2, and He, as measured somewhat away from the reaction zone within the laser cavity, were 3, 3, and 925 mTorr, respectively, for maximum signal strengths. (1 Torr corresponds to 133 Pa.) These conditions gave a bright blue flame in the center of the laser cavity. Helium pressures were an order of magnitude lower for the Lamb-dip hyperfine measurements.

Examples of the spectra obtained (in derivative display) are shown in Figs. 3 to 5,

TABLE III

Magnetic Field Measurements, Assignments, Hyperfine Splittings, and Observed-minus-Calculated Values for the $(J' \leftarrow J'') = (\frac{5}{2} \leftarrow \frac{3}{2})$ and $(\frac{7}{2} \leftarrow \frac{5}{2})$ Transitions of CH

M_J'	M_J''	H[a]	O-C[b]	∂E/∂H[c]	ΔH[d]	O-C[e]
180.7 μm		$F_{1e}(2) \leftarrow F_{1e}(1)$			5/2 ← 3/2	
+3/2	+3/2	3.2185	-0.0	-0.7350	-	-
+1/2	+3/2	1.6699	+0.2	-1.4382	6.7	+0.0
-1/2	+1/2	2.5985	-0.1	-0.9144	10.8	-0.0
-3/2	-1/2	5.9153	+0.0	-0.3817	26.2	+0.0
180.7 μm		$F_{1f}(2) \leftarrow F_{1f}(1)$			5/2 ← 3/2	
-3/2	-3/2	2.1857	-0.3	+0.8007	-7.2	+0.0
-1/2	-1/2	5.7456	+0.1	+0.3415	-	-
-1/2	-3/2	1.1614	+0.9	+1.4934	-1.8	-0.1
+1/2	-1/2	1.7752	-0.3	+0.9820	1.4	+0.0
+3/2	+1/2	3.7701	-0.0	+0.4720	11.1	-0.0
118.6 μm[f]		$F_{1e}(3) \leftarrow F_{1e}(2)$			7/2 ← 5/2	
+5/2	+5/2	8.242	+4.9	-0.4359	5.3	-0.1
+3/2	+3/2	17.147	-2.6	-0.1612	-	-
+3/2	+5/2	4.116	+3.4	-0.9231	12.5	+0.2
+1/2	+3/2	5.275	+3.2	-0.7108	13.6	-0.3
-1/2	+1/2	7.377	+2.5	-0.4920	17.1	+0.3
-3/2	-1/2	12.694	-2.1	-0.2443	26.7	-0.1
118.6 μm[f]		$F_{1f}(3) \leftarrow F_{1f}(2)$			7/2 ← 5/2	
-5/2	-5/2	4.258	+3.9	+0.6043	-	-
-3/2	-3/2	6.628	+2.3	+0.4118	-	-
-1/2	-1/2	13.221	-7.9	+0.2572	11.0	-0.1
-3/2	-5/2	2.316	+3.9	+1.0778	-	-
-1/2	-3/2	2.924	+4.6	+0.8559	4.8	-0.1
+1/2	-1/2	3.968	+6.6	+0.6331	7.3	+0.6
+3/2	+1/2	6.171	+1.0	+0.4080	11.1	+0.4
+5/2	+3/2	14.173	-0.5	+0.1741	-	-
118.8 μm[g]		$F_{1e}(3) \leftarrow F_{1e}(2)$			7/2 ← 5/2	
+3/2	+5/2	10.1149	+2.2	-0.8037	12.5	-0.2
+1/2	+3/2	13.2780	-1.6	-0.5836	14.4	+0.2
118.8 μm		$F_{1f}(3) \leftarrow F_{1f}(2)$			7/2 ← 5/2	
+5/2	+5/2	5.4669	-2.5	-0.4685	-6.2	-0.5
+3/2	+3/2	10.3155	+1.7	-0.2162	-14.7	+0.2
+3/2	+5/2	2.7731	-1.4	-0.9586	1.3	+0.1
+1/2	+3/2	3.5347	-1.6	-0.7469	2.2	-0.1
-1/2	+1/2	4.8822	-1.4	-0.5325	4.2	-0.0
-3/2	-1/2	7.9731	+1.1	-0.3083	8.6	-0.4

[a] Magnetic field measurement in [kG] at the center of each two-line hyperfine pattern.

[b] Observed-minus-Calculated values in [G] from fits of each of the six M_J patterns in this table to Eq. (18); $\nu_{mismatch}$ and (g_J') were both varied, except for the fifth pattern.

[c] Value of (∂E'/∂H-∂E"/∂H) in [MHz/G] at the center of each two-line hyperfine pattern, obtained from fits of the M_J structure.

[d] Measured separation in [G] of the two hyperfine components of each line. Blank entries indicate splittings too small to resolve. Signs have been determined as described in the text, so that the definition of ΔH in Eq. (28) is valid.

[e] Observed-minus-Calculated values in [G] from fits of four sets of hyperfine splittings to Eq. (28). (Hyperfine splittings from the 118.6 and 118.8 um patterns corrresponding to the same free-molecule transition were combined and fit simultaneously.)

[f] Central magnetic field values here were taken from the literature (3); hyperfine splittings were taken from unpublished work of A. H. Curran, K. M. Evenson and H. E. Radford.

[g] The M_J structure here was fit to Eq. (18), varying only $\nu_{mismatch}$ (see Table IV).

which illustrate a 180.7 μm survey spectrum, a fully resolved 554.4 μm Doppler broadened hyperfine pattern, and a 180.7 μm sub-Doppler Lamb-dip hyperfine measurement.

All magnetic field measurements obtained in this work, together with assignments and other quantities to be discussed in later sections, are presented in Tables II and III.

III. THEORETICAL MODEL

In this section we shall: (i) define the case (a_β) basis set functions used to carry out the theoretical calculations, (ii) discuss the three parts of the molecular Hamiltonian, corresponding to the (large) rotational energy effects, the (intermediate-size) magnetic splittings, and the (small) hyperfine splittings, and (iii) present some simple expressions for various quantities, valid when $A = 2B$. A more detailed pedagogical discussion of material used in this section may be found in (*12*).

Basis Set Functions

The basis set functions used here are characterized by eight angular momentum quantum numbers

$$|\Lambda S\Sigma; \Omega J M_J; I M_I\rangle, \tag{1}$$

and are quite standard for the problem at hand. The quantum numbers S, J, and I represent the total electron spin, the total molecular angular momentum excluding nuclear spin, and the nuclear spin of the proton, respectively. The quantum numbers Λ, Σ, and Ω represent projections along the internuclear axis of the electron orbital angular momentum, the electron spin, and the sum of electron orbital and spin angular momentum, respectively. The quantum numbers M_J and M_I represent projections along the laboratory-fixed Z axis of $\mathbf{J}$ and $\mathbf{I}$. For the $X^2\Pi$ state of CH, $S = \frac{1}{2}$, $I = \frac{1}{2}$, and Λ, Σ, M_I take on only the values ± 1, $\pm\frac{1}{2}$, $\pm\frac{1}{2}$, respectively.

The functions (1) are sometimes described as case (a_β) functions (*13*). The (a) indicates that the electron spin is projected along the molecule-fixed z axis (internuclear axis); the subscript β indicates that the nuclear spin is projected along the laboratory-fixed Z axis. (In this paper, capital letters X, Y, Z denote laboratory-fixed axes; lower-case letters x, y, z denote molecule-fixed axes.)

Hamiltonian Operator and Matrix Elements

The Hamiltonian operator for the physical effects under consideration can be divided for conceptual and computational convenience into three parts.

$$\mathcal{H} = \mathcal{H}_r + \mathcal{H}_m + \mathcal{H}_n. \tag{2}$$

The spin–rotation Hamiltonian $\mathcal{H}_r$ can be written (*12*) in terms of molecule-fixed components of the angular momentum operators $\mathbf{L}$, $\mathbf{S}$, $\mathbf{J}$, and the three molecular parameters A (spin–orbit coupling constant), B (rotational constant), D (centrifugal distortion constant).

$$\mathcal{H}_r = +AL_zS_z + B[(J_x - S_x)^2 + (J_y - S_y)^2] - D[(J_x - S_x)^2 + (J_y - S_y)^2]^2. \tag{3}$$

The magnetic Hamiltonian $\mathcal{H}_m$ can be written (*14*) in terms of laboratory-fixed components of the operators L, S, I, the magnetic field strength H, and the universal constants $\mu_B = 1.399612$ MHz/G (Bohr magneton), $\mu_n = 0.762253$ MHz/kG (nuclear magneton), $g_e = 2.00232$ (g-value of the free electron spin), $g_I = 5.58569$ (g-value of the proton).

$$\mathcal{H}_m = +\mu_B(L_Z + g_e S_Z)H - g_I \mu_n I_Z H. \tag{4}$$

The hyperfine Hamiltonian $\mathcal{H}_A$ can be written, following Frosch and Foley (*13*), in terms of molecule-fixed components of the operators L, S, I (or the corresponding ladder operators $L_\pm \equiv L_x \pm iL_y$, etc.), and the four molecular hyperfine constants a, b, c, d.

$$\mathcal{H}_A = aI_zL_z + b\mathbf{I}\cdot\mathbf{S} + cI_zS_z + \tfrac{1}{2}d[L_-^2I_+S_+ + L_+^2I_-S_-]. \tag{5}$$

Because of the choice of good quantum numbers in the basis set (1), matrix elements of all operators in Eqs. (3–5) except L_Z and S_Z in Eq. (4) and I_+, I_-, and I_z in Eq. (5) can be found from standard elementary angular momentum considerations (*12*). Matrix elements of the first two (last three) of the five operators mentioned above can conveniently be obtained after expressing them in terms of molecule-fixed (laboratory-fixed) vector components by means of the direction cosine matrix α.

$$L_Z = \alpha_{Zx}L_x + \alpha_{Zy}L_y + \alpha_{Zz}L_z \tag{6a}$$

$$I_z = \alpha_{Xz}I_X + \alpha_{Yz}I_Y + \alpha_{Zz}I_Z, \tag{6b}$$

where the analog of Eq. (6a) holds for S_Z, the analog of Eq. (6b) for I_y and I_z. Matrix elements for the direction cosines are well known (*14*). For the basis set (1), these matrix elements must be considered to be functions of J, Ω, and M_J (*12*). When evaluating matrix elements satisfying $\Delta J = 0$, the particularly simple operator equivalent

$$\alpha_{Rs} \rightarrow J_R J_s/J(J+1), \tag{7}$$

where $R = X$, Y, or Z and $s = x$, y, or z, is often convenient.

Simple Expressions Valid when $A = 2B$

The ratio A/B for the $X^2\Pi$ state of CH, as found in the literature, is 1.97 (*1*) or 2.00 (*2*). It is thus frequently convenient to make initial estimates of various quantities for CH with the help of simple expressions which can be derived when $A = 2B$.

Following (*12*), we can easily obtain rotational energies and wavefunctions from the basis set (1) and the Hamiltonian (3) with $A = 2B$ and $D = 0$. The energies, which are independent of the e, f parity subscripts because Λ-doubling effects have not been included in Eq. (3), take the forms

$$\begin{aligned} F_2(1) &= 0 \\ F_2(N \geq 2) &= B[N(N+1) - 1] - B[N - (N^2 - 1)^{\frac{1}{2}}] \\ F_1(N \geq 1) &= B[N(N+1) - 1] + B[(N+1) - (N^2 + 2N)^{\frac{1}{2}}]. \end{aligned} \tag{8}$$

These expressions, apart from $F_2(1)$, only differ by approximately $B/2N$ from the case (b) values of $B[N(N+1) - 1]$. For a particular choice of phase factors (*12*), we can

write the corresponding rotational wavefunctions as

$$|F_{2e,f}(1)\rangle = 2^{-\frac{1}{2}}\{|+1,\tfrac{1}{2},-\tfrac{1}{2};+\tfrac{1}{2},\tfrac{1}{2},M_J\rangle \mp |-1,\tfrac{1}{2},+\tfrac{1}{2};-\tfrac{1}{2},\tfrac{1}{2},M_J\rangle\}$$

$$\begin{aligned}|F_{2e,f}(N\geq 2)\rangle = 4^{-\frac{1}{2}}\{&[|+1,\tfrac{1}{2},+\tfrac{1}{2};+\tfrac{3}{2},N-\tfrac{1}{2},M_J\rangle - |+1,\tfrac{1}{2},-\tfrac{1}{2};+\tfrac{1}{2},N-\tfrac{1}{2},M_J\rangle]\\ &\mp [|-1,\tfrac{1}{2},-\tfrac{1}{2};-\tfrac{3}{2},N-\tfrac{1}{2},M_J\rangle\\ &\qquad - |-1,\tfrac{1}{2},+\tfrac{1}{2};-\tfrac{1}{2},N-\tfrac{1}{2},M_J\rangle]\}\end{aligned} \quad (9)$$

$$\begin{aligned}|F_{1e,f}(N\geq 1)\rangle = 4^{-\frac{1}{2}}\{&[|+1,\tfrac{1}{2},+\tfrac{1}{2};+\tfrac{3}{2},N+\tfrac{1}{2},M_J\rangle + |+1,\tfrac{1}{2},-\tfrac{1}{2};+\tfrac{1}{2},N+\tfrac{1}{2},M_J\rangle]\\ &\mp [|-1,\tfrac{1}{2},-\tfrac{1}{2};-\tfrac{3}{2},N+\tfrac{1}{2},M_J\rangle\\ &\qquad + |-1,\tfrac{1}{2},+\tfrac{1}{2};-\tfrac{1}{2},N+\tfrac{1}{2},M_J\rangle]\},\end{aligned}$$

where proton nuclear spin functions have been omitted. The latter can be supplied simply by multiplying the left- and right-hand sides of Eqs. (9) by $|IM_I\rangle$. It is easily seen that the rotational wavefunctions (9), except for $F_{2e,f}(1)$, represent equal mixtures of $^2\Pi_{\frac{1}{2}}$ basis set functions ($\Omega = \pm\frac{3}{2}$) with $^2\Pi_{\frac{1}{2}}$ basis set functions ($\Omega = \pm\frac{1}{2}$).

We now use the magnetic Hamiltonian (4), with the substitutions of Eqs. (6) and (7), and the rotational wavefunctions (9) to obtain first-order magnetic field corrections $E_m^{(1)}$ to the rotational energies (8). These corrections, which are appropriate when $(\mu_B HN/B) < 0.1$, take the form

$$E_m^{(1)} = -g_J\mu_B M_J H, \quad (10)$$

where g_J is independent of the e, f parity subscripts and has the values

$$\begin{aligned}g_J[F_2(1)] &= -(1-\tfrac{1}{2}g_s)/2J(J+1)\\ g_J[F_2(N\geq 2)] &= -\{2+\tfrac{1}{2}g_s - g_s[(J-\tfrac{1}{2})(J+\tfrac{3}{2})]^{\frac{1}{2}}\}/2J(J+1)\\ g_J[F_1(N\geq 1)] &= -\{2+\tfrac{1}{2}g_s + g_s[(J-\tfrac{1}{2})(J+\tfrac{3}{2})]^{\frac{1}{2}}\}/2J(J+1).\end{aligned} \quad (11)$$

Nuclear spin contributions to the magnetic energies (10) are omitted, since they are smaller than neglected higher order contributions from the electron spin.

By substituting Eqs. (6) and (7) in the hyperfine Hamiltonian (5), and taking expectation values of all operators involving *molecule-fixed* vector components over the rotational wavefunctions (9), we obtain a convenient operator equivalent for calculating first-order hyperfine corrections to the energy.

$$\mathcal{H}_h \rightarrow h(I_X J_X + I_Y J_Y + I_Z J_Z) = h(\mathbf{I}\cdot\mathbf{J}), \quad (12)$$

where the effective hyperfine interaction constant h is given by

$$\begin{aligned}h[F_{2e,f}(1)] &= \{+2a-(b+c)\mp 2d\}/4J(J+1)\\ h[F_{2e,f}(N\geq 2)] &= \{+4a+(b+c)\mp d(J+\tfrac{1}{2}) - 2b[(J-\tfrac{1}{2})(J+\tfrac{1}{2})]^{\frac{1}{2}}\}/4J(J+1)\\ h[F_{1e,f}(N\geq 1)] &= \{+4a+(b+c)\mp d(J+\tfrac{1}{2}) + 2b[(J-\tfrac{1}{2})(J+\tfrac{1}{2})]^{\frac{1}{2}}\}/4J(J+1),\end{aligned} \quad (13)$$

if we consider the ladder operators L_+^2 and L_-^2 in Eq. (5) to be normalized such that $\langle\Lambda = \pm 1|L_\pm^2|\Lambda = \mp 1\rangle = +1$ in the basis set (1).

Two simple hyperfine energy level patterns can be obtained from Eq. (12),

$$E_h^{(1)} = \tfrac{1}{2}h[F(F+1) - J(J+1) - I(I+1)] \quad (14a)$$

$$E_h^{(1)} = hM_I M_J. \quad (14b)$$

Equation (14a) is valid when the magnetic field $H = 0$, with the quantum number F obtained from I and J by vector addition. Equation (14b) is valid when

$$N|h| \ll |g_J|\mu_B H \ll B/N. \tag{15}$$

IV. DETAILS OF THE FIT OF THE M_J STRUCTURE

The coarse structure of laser magnetic resonance spectra observed in this work (see Fig. 3) arises from transitions between Zeeman split components $M_J' \leftarrow M_J''$ of pure rotational transitions $(N', J') \leftarrow (N'', J'')$ in the CH molecule. Quantum number assignments for individual M_J transitions were easily determined from known wavenumbers for the far infrared laser lines (*5, 6, 7, 8*), literature values for the CH rotational energy differences (*2*), and the simple first-order g_J expressions in Eqs. (11).

The steps in the least squares fitting procedure used to reduce the data were as follows: (i) a preliminary fit of the M_J structure was carried out, making no attempt to correct for hyperfine splitting effects; (ii) some information from the preliminary M_J fit was used in a separate fit of the hyperfine splittings; (iii) some information from the hyperfine fit was used to produce hypothetical field positions corresponding to M_J transitions free from hyperfine splitting effects, and these hypothetical M_J transitions were refit. Steps (ii) and (iii) were iterated until consistency was achieved. All three of these steps require some additional theoretical manipulation. In this section we discuss only steps (i) and (iii) .

Hamiltonian Matrix and Least Squares Equations

Since the hyperfine corrections determined in the next section take into account all contributions from the proton nuclear spin, we consider in this section only an electronic magnetic Hamiltonian $\mathcal{H}_{mf}$, obtained from Eq. (4) by omitting the term in I_z,

$$\mathcal{H}_{mf} = +(L_z + g_s S_z)\mu_B H. \tag{16}$$

Nonvanishing matrix elements of this operator obey the selection rules $\Delta M_J = 0$ and $\Delta J = 0, \pm 1$. We set up the Hamiltonian matrix representing magnetic interaction of a given level (N, J, M_J) with other levels satisfying these selection rules in three steps. First we determine a set of zero-field rotational wavefunctions and energy levels for CH using Eqs. (1) and (3) and values of A, B, and D from the literature (*1, 2*). Then, using these wavefunctions, a 2×2 matrix is formed by evaluating matrix elements of $\mathcal{H}_{mf}$ within the pair $|F_1(N)\rangle$, $|F_2(N)\rangle$ characterized by a given value of N; the energy separation at zero magnetic field of these two close-lying levels is set equal to the observed value (*2*). Finally, Van Vleck corrections (*12*) are made to each of the four elements of this 2×2 matrix, using the Hamiltonian operator $\mathcal{H}_{mf}$ and taking into account interactions of the rotational wavefunctions $|F_1(N)\rangle$ and $|F_2(N)\rangle$ with the rotational wavefunctions $|F_1(N+1)\rangle$, $|F_1(N-1)\rangle$, $|F_1(N-2)\rangle$, $|F_2(N+2)\rangle$, $|F_2(N+1)\rangle$ and $|F_2(N-1)\rangle$ from step one. The Van Vleck corrected 2×2 matrix is then diagonalized to obtain magnetic energies $E_{mf}(H)$ for various magnetic fields.

The above procedure takes into account the necessary magnetic interactions *within* the $^2\Pi$ state. As is well known (*15*), the operators L_x and L_y induce a slight contamination of $^2\Pi$ states by $^2\Sigma$ and $^2\Delta$ states, which gives rise to the Λ-doubling effects in CH. This

same contamination also gives rise to slight changes in the magnetic properties of the rotational levels. In this work these slight changes are introduced by adding a small *empirical* correction term $-\Delta g_J \mu_B M_J H$.

The final energy expression $E(H)$ for a given (N, J, M_J) state in an external magnetic field, for use in the least squares fits of the M_J structure, has the form

$$E(H) = E_{m\ell}(H) - E_{m\ell}(0) - \Delta g_J \mu_B M_J H. \tag{17}$$

TABLE IV

Parameters from Least Squares Fits[a] of the M_J Structure

Transition	λ [μm][b]	σ [G][c]	$\Delta g_J'$[d]	$\Delta g_J''$	$\nu_{mismatch}$ [cm^{-1}][d]
$F_{1e}(1) \leftarrow F_{2e}(1)$[e]	567.9	1.3	-0.00217[f]	-0.00507[g]	-0.29754(2)
$v = 0$	561.3	0.0	-0.00217	-0.00507	-0.08882(0)
	554.4	0.1	-0.00217	-0.00507	+0.13380(0)
$F_{1e}(1) \leftarrow F_{2e}(1)$[e]	567.9	3.9	+0.00817[f]	-0.00500[g]	-0.24414(5)
$v = 1$	561.3	1.2	+0.00817	-0.00500	-0.03559(2)
	554.4	1.5	+0.00817	-0.00500	+0.18720(2)
$F_{1f}(1) \leftarrow F_{2f}(1)$[e]	567.9	0.5	-0.00557[f]	+0.00010[g]	-0.16309(1)
$v = 0$	561.3	0.5	-0.00557	+0.00010	+0.04567(1)
	554.4	1.1	-0.00557	+0.00010	+0.26826(2)
$F_{1f}(1) \leftarrow F_{2f}(1)$[e]	567.9	0.4	+0.00551[f]	-0.00008[g]	-0.11738(1)
$v = 1$	561.3	1.6	+0.00551	-0.00008	+0.09128(2)
	554.4	4.0	+0.00551	-0.00008	+0.31398(6)
$F_{1e}(2) \leftarrow F_{1e}(1)$[h]	180.7	0.2	-0.00148(1)	-0.00217[i]	-0.08092(0)
$F_{1f}(2) \leftarrow F_{1f}(1)$[h]	180.7	0.6	-0.00422(3)	-0.00557[i]	+0.05741(1)
$F_{1e}(3) \leftarrow F_{1e}(2)$[h]	118.6	4.0	-0.00135(2)	-0.00148[j]	-0.13301(2)
	118.8	2.7	-0.00135[k]	-0.00148	-0.30546(4)
$F_{1f}(3) \leftarrow F_{1f}(2)$[h]	118.6	5.2	-0.00399(2)	-0.00422[j]	+0.08094(3)
	118.8	2.0	-0.00404(2)	-0.00422	-0.09160(1)

[a] Using Eqs. (17) and (18), and molecular constants A = 28.382, B = 14.191 (2), and D = 0.00143 (1) cm^{-1}. An observed value (2) for the appropriate $F_1(N)$-$F_2(N)$ spacing was also used in setting up each 2 x 2 matrix, as described in the text.

[b] Laser wavelength used to record spectrum.

[c] Standard deviation of the fit.

[d] Numbers in parentheses indicate one standard deviation of the last digit given, as obtained from the least squares program.

[e] Data and Observed-minus-Calculated values in Table II.

[f] Adjusted to eliminate discrepancies in values of $\nu_{molecule}$ determined from spectra of the same (3/2 ← 1/2) transition recorded with λ = 554.4 and 567.9 μm.

[g] Determined directly from least squares fits of the (3/2 ← 1/2) hyperfine patterns.

[h] Data and Observed-minus-Calculated values in Table III.

[i] Fixed at the adjusted value from the (3/2 ← 1/2) fits.

[j] Fixed at the least squares value from the (5/2 ← 3/2) fits.

[k] Fixed at the least squares value from the 118.6 μm. $F_{1e}(3) \leftarrow F_{1e}(2)$ fit.

The first term on the right is obtained by diagonalizing the Van Vleck corrected 2×2 matrices; the second simply scales the energy so that $E(H = 0) = 0$ for the (N, J) rotational level under consideration; and the third term is the empirical correction.

Least squares fits were carried out by minimizing the squares of the function $H_{obs} - H_{calc}$, which can be shown to take the form

$$H_{obs} - H_{calc} = [E'(H_{obs}) - E''(H_{obs}) - \nu_{mismatch}]/[\partial E'/\partial H - \partial E''/\partial H]_{H=H_{obs}}, \quad (18)$$

when written in terms of upper and lower state energies $E'(H)$ and $E''(H)$ as defined in Eq. (17), and the quantity

$$\nu_{mismatch} = \nu_{laser} - \nu_{molecule}, \quad (19)$$

where ν_{laser} represents the wavenumber of the far infrared laser used to record the magnetic resonance spectrum and $\nu_{molecule}$ represents the wavenumber of one Λ-doublet of the molecular transition $(N', J') \leftarrow (N'', J'')$ in field-free space. In a given least squares fit, only $M_J' \leftarrow M_J''$ transitions belonging to this one field-free molecular transition are included. During a fit, one or more of the three quantities $\nu_{mismatch}$, $\Delta g_J'$, and $\Delta g_J''$ occurring in Eqs. (17) and (18) are allowed to vary.

Analysis of the M_J Structure

Preliminary fits of the M_J patterns in Table III and non-hyperfine-corrected patterns in Table II were carried out using Eq. (18) with $\Delta g_J' = \Delta g_J'' = 0$. Initial estimates for $\nu_{mismatch}$, the only quantity varied in these fits, were obtained from graphical displays of upper and lower state Zeeman splittings, as predicted by Eqs. (10) and (11) in the section on "simple expressions valid when $A = 2B$."

The fit of each pattern in Table II of hypothetical M_J transitions free from hyperfine splitting effects, as determined in Section V below, and of each M_J pattern in Table III, was also carried out using Eq. (18) with $\Delta g_J'$ and $\Delta g_J''$ permitted to vary. Treatment of the empirical correction term in Δg_J was somewhat different for levels with $J = \frac{1}{2}$,

TABLE V

Low-lying Rotational Energy Levels of CH

N	J	Energy [cm^{-1}]		Λ-doubling = $\Delta\nu_{ef}$ [cm^{-1}]	
		This work	Other	This work	Other
1	1/2	0.0	0.0	-	-0.1108[a], -0.1135[b]
1	3/2	17.8376(2)[c]	17.836[b]	+0.0237(2)[c]	+0.018[b]
2	5/2	73.1773(3)	73.180[b]	+0.1620(3)	+0.159[b]
3	7/2	157.5267(4)	157.536[b]	+0.3759(4)	+0.373[b]

[a] Reference (4). Used here to calculate the higher-J Λ-doublings.

[b] Reference (2).

[c] Numbers in parentheses indicate the authors' estimates of overall (statistical plus systematic) uncertainties in the last digit.

levels with $J = \frac{3}{2}$, and levels with $J = \frac{5}{2}$ or $\frac{7}{2}$, as described below. Values for the parameters varied in the least squares fits of this section and for the molecular energy levels determined are summarized in Tables IV and V, respectively.

The parameter Δg_J for each of the two Λ-doublet components of the $J = \frac{1}{2}$ rotational state was determined directly from least squares fits of $(\frac{3}{2} \leftarrow \frac{1}{2})$ *hyperfine* patterns in Section V. This was possible because the extremely small Zeeman splittings exhibited when $J = \frac{1}{2}$ lead to hyperfine patterns which are strongly dependent on Δg_J, as can be seen from Eq. (27).

Values of Δg_J for the $J = \frac{3}{2}$ Λ-doublet components were adjusted by hand to eliminate discrepancies in the values of ν_{molecule} obtained from separate fits to Eq. (18) of the same molecular transition recorded with different laser wavelengths near 560 μm. In such least squares fits of the M_J structure of either $F_{1e}(1) \leftarrow F_{2e}(1)$ or $F_{1f}(1) \leftarrow F_{2f}(1)$ transitions, only ν_{mismatch} was varied, $\Delta g_J''$ having been determined as described in the preceding paragraph. When $\Delta g_J \equiv 0$ for the $J = \frac{3}{2}$ Λ-components, discrepancies in ν_{molecule} are as large as 0.004 cm^{-1}; when $\Delta g_J'$ has the values given in Table IV, these discrepancies are reduced to 0.0001 cm^{-1}. The first of two checks on this empirical correction procedure is provided by the fact that the same value of $\Delta g_J'$ which removes the discrepancy between values of ν_{molecule} obtained from the shortest and longest laser wavelengths (554.4 and 567.9 μm) also removes the discrepancy for the middle laser wavelength (561.3 μm).

Values of Δg_J for the Λ-doublet components of the $J = \frac{5}{2}$ and $J = \frac{7}{2}$ rotational states were determined from separate least squares fits of the M_J structure of the $(\frac{5}{2} \leftarrow \frac{3}{2})$ and $(\frac{7}{2} \leftarrow \frac{5}{2})$ transitions, respectively, to Eq. (18), varying only ν_{mismatch} and $\Delta g_J'$. In the first fit, $\Delta g_J''$ $(J'' = \frac{3}{2})$ was held fixed at the value obtained from the procedure of the preceding paragraph. In the second fit, $\Delta g_J''$ $(J'' = \frac{5}{2})$ was held fixed at the value obtained from the procedure of the preceding sentence.

The second check on this empirical correction procedure is now possible, since we have fit the $F_{1f}(3) \leftarrow F_{1f}(2)$ $(\frac{7}{2} \leftarrow \frac{5}{2})$ spectrum recorded at both 118.6 μm and 118.8 μm. Consistency requires that the same $\Delta g_J'$ and ν_{molecule} values be obtained in both fits. Indeed, as indicated in Table IV, the $\Delta g_J'$ values agree to 0.00005 (1.3%); the values of ν_{mismatch} in Table IV yield values for ν_{molecule} which agree to 0.0001 cm^{-1}. An identical check cannot be obtained for the $F_{1e}(3) \leftarrow F_{1e}(2)$ transition, since the 118.8 μm spectrum contains only two lines. Nevertheless, by fixing $\Delta g_J'$ at its 118.6 μm value, and varying only ν_{mismatch} in Eq. (18), we obtain a value of ν_{molecule} which also agrees with its 118.6 μm counterpart to 0.0001 cm^{-1}. Thus, even though at present the values of the small correction parameters Δg_J cannot be deduced theoretically, we believe the empirical correction procedure is justified and leads to correct results.

V. DETAILS OF THE FIT OF THE HYPERFINE STRUCTURE

The finer structure of the laser magnetic resonance spectra observed in this work (see Figs. 4 and 5) arises from the hyperfine splittings superimposed on each M_J level. To avoid transferring the larger errors associated with least squares fits of the coarser M_J structure into fits of the hyperfine splittings, we choose here to fit the hyperfine structure by itself. We thus consider only step (ii) of the procedure described in section IV. From this step we obtain molecular hyperfine constants, which are used in turn to

calculate hypothetical magnetic field values for M_J transitions which are free from all effects caused by the proton nuclear spin.

Hamiltonian Matrix and Energy Expressions

Since we wish to take into account here all observed effects associated with the proton nuclear spin, we consider a nuclear hyperfine Hamiltonian $\mathcal{H}_{hn}$ obtained by adding the last term in Eq. (4) to Eq. (5).

$$\mathcal{H}_{hn} = +aI_zL_z + b\mathbf{I}\cdot\mathbf{S} + cI_zS_z + \tfrac{1}{2}d[L_-^2I_+S_+ + L_+^2I_-S_-] - g_I\mu_nI_ZH. \quad (20)$$

Nonvanishing matrix elements of this operator satisfy the selection rule $\Delta M_F \equiv \Delta M_I + \Delta M_J = 0$.

We consider matrix elements of $\mathcal{H}_{hn}$ in a basis set which includes spin–rotational effects together with first-order magnetic field corrections, as defined by the equation

$$|F_i(N);\, M_I,\, M_J;\, \epsilon_i\rangle \equiv [|F_i(N),\, M_J\rangle + \epsilon_i|F_{3-i}(N),\, M_J\rangle]|I,\, M_I\rangle. \quad (21)$$

The subscripts i and $3 - i$, where $i = 1$ or 2, are simply a convenient shorthand notation for indicating $F_1(N)$ and $F_2(N)$ levels. The quantities $|F_i(N), M_J\rangle$ are rotational wavefunctions obtained from Eqs. (1) and (3) for $A = 2B$ and $D = 0$, as given in Eqs. (9). The small coefficients ϵ_i, which are functions of i, N, M_J, and H, result from first-order magnetic-field mixing of the two states separated by an energy of order B/N.

$$\epsilon_i = \langle F_{3-i}(N),\, M_J|\mathcal{H}_{ms}|F_i(N),\, M_J\rangle/[F_i(N) - F_{3-i}(N)]. \quad (22)$$

In addition to the approximations made above in defining the basis set, we consider matrix elements of $\mathcal{H}_{hn}$ only between M_I and M_J components of a given perturbed $F_i(N)$ level on the left of Eq. (21).

The simplest hyperfine splitting patterns are obtained from Eqs. (20–21) in the "high field limit," which occurs when the Zeeman splittings between different M_J levels of a given (N, J) rotational state are large compared to the hyperfine interaction energies. Under these circumstances, only $\Delta M_J = 0$ matrix elements of $\mathcal{H}_{hn}$ need be considered, and we obtain for the hyperfine contribution to the energy of the state $|F_i(N);\, M_I,\, M_J;\, \epsilon_i\rangle$

$$E_{hn} = kM_IM_J + kHM_I[1 - M_J^2/(N + \tfrac{1}{2})^2] - g_I\mu_nM_IH, \quad (23)$$

where h is given for $F_i(N)$ in Eqs. (13) and k, which is independent of M_I and M_J, may be evaluated for $F_i(N)$ using the simple product basis set.

$$k = 2\epsilon_i\{\langle I,\, M_I|\langle F_{3-i}(N),\, M_J|\mathcal{H}_{hn}|F_i(N),\, M_J\rangle|I,\, M_I\rangle\}/ \{HM_I[1 - M_J^2/(N + \tfrac{1}{2})^2]\}. \quad (24)$$

The high-field-limit expression (23) is valid when $J \geq \frac{1}{2}$ and H is greater than a few hundred gauss.

Table I indicates that g_J is very small for $J = \frac{1}{2}$. Consequently, for the magnetic fields used in this work Zeeman splittings within the $J = \frac{1}{2}$ state are never large compared to the hyperfine energies. Under these circumstances, both $\Delta M_J = 0$ and $\Delta M_J = \pm 1$ matrix elements of $\mathcal{H}_{hn}$ in the basis set (21) must be considered. We find that when $M_F \equiv M_I + M_J = \pm 1$ in the $J = \frac{1}{2}$ state, the hyperfine energy contribution

is still given by Eq. (23). When $M_F = 0$, the two possible states (i.e., $M_I = -M_J = \pm\frac{1}{2}$) interact, and a 2×2 matrix of the operator

$$\mathcal{H}_{hn} + (\mathcal{H}_{ms})_{ef} \tag{25}$$

in the basis set (21) must be considered. Diagonal matrix elements of $\mathcal{H}_{hn}$ are given by Eq. (23); off-diagonal elements have the value $+\frac{1}{2}h$. Matrix elements of the effective magnetic Hamiltonian $(\mathcal{H}_{ms})_{ef}$, which are introduced only to take account of the Zeeman splitting of the $M_J = \pm\frac{1}{2}$ levels in the absence of hyperfine interactions, are diagonal in M_J and can be represented phenomenologically by the expression

$$-[(g_J)_{ef} + fH^2]\mu_B M_J H, \tag{26}$$

which allows for third-order contributions to the splitting comparable in size to the very small first-order contribution. Hyperfine energies for $M_F = 0$ states of $J = \frac{1}{2}$ obtained by diagonalizing the 2×2 matrix take the form

$$E_{hn} = -\tfrac{1}{4}h \pm \tfrac{1}{2}\{h^2 + [(g_J)_{ef}\mu_B + f\mu_B H^2 - g_I\mu_n + 8k/9]^2H^2\}^{\frac{1}{2}}. \tag{27}$$

Least-Squares Equations

When the high field limit applies to both the upper M_J' and lower M_J'' states, M_I is a good quantum number and allowed transitions satisfy $\Delta M_I = 0$. We then find from Eq. (23) that the separation ΔH in magnetic field between the two components of an observed hyperfine doublet satisfies the relation

$$\begin{aligned}\Delta H \equiv\ & H(M_J', M_J''; M_I = +\tfrac{1}{2}) - H(M_J', M_J''; M_I = -\tfrac{1}{2}) \\ =\ & \{-h'M_J' + h''M_J'' - k'H[1 - (M_J')^2/(N' + \tfrac{1}{2})^2] \\ & + k''H[1 - (M_J'')^2/(N'' + \tfrac{1}{2})^2]\}/[\partial E'/\partial H - \partial E''/\partial H],\end{aligned} \tag{28}$$

where the $\partial E/\partial H$ represent derivatives of the magnetic energies $E(H)$ of Eq. (17) evaluated at the center of the hyperfine doublet. These derivatives are determined from fits of the M_J structure (Section IV), and are not allowed to vary in a hyperfine fit. Least squares fits of the hyperfine structure when $J'' \geq \frac{3}{2}$ were carried out by minimizing the squares of $(\Delta H_{obs} - \Delta H_{calc})$ with respect to variation of one or more of the parameters h', k', h'', and k'' in Eq. (28).

When $J'' = \frac{1}{2}$, the high field limit does not apply (as illustrated by the hyperfine pattern in Fig. 4, containing three components rather than the two permitted by the selection rule $\Delta M_I = 0$), and a somewhat more complicated fitting procedure must be adopted. For a small region about some central magnetic field H_0, i.e., for the region containing some hyperfine pattern, one can parameterize the magnetic field positions $H(M_I', M_J'; M_I'', M_J'')$ of the hyperfine components as follows,

$$H(M_I', M_J'; M_I'', M_J'') = H_0(M_J') - [E'_{hn} - E''_{hn}]/[\partial E'/\partial H - \partial \bar{E}''/\partial H]. \tag{29}$$

M_J' is assumed fixed in this expression; M_I', M_I'' and M_J'' all take on the possible values $\pm\frac{1}{2}$. E'_{hn} is the hyperfine energy of a $J' = \frac{3}{2}$ level and is given by Eq. (23); E''_{hn} is the hyperfine energy of a $J'' = \frac{1}{2}$ level and is given by Eqs. (23) plus (26) or by Eq. (27). The derivatives $\partial E'/\partial H$ and $\partial \bar{E}''/\partial H$, which represent $\partial E'(H, M_J')/\partial H$ at $H = H_0$ and $\frac{1}{2}[\partial E''(H, M_J'' = +\frac{1}{2})/\partial H + \partial E''(H, M_J'' = -\frac{1}{2})/\partial H]$ at $H = H_0$,

respectively, as obtained from the M_J fit to Eq. (18), are not allowed to vary here. Least squares fits of the hyperfine structure of the $J' = \frac{3}{2} \leftarrow J'' = \frac{1}{2}$ transitions were carried out by minimizing the squares of $H_{obs} - H(M_I', M_J'; M_I'', M_J'')$ with respect to variation of one or more of the parameters H_0, h', k', $(g_J'')_{eff}$, f'', h'', and k'' in Eq. (29).

It can be seen after some reflection that the value of $\Delta g_J''$ required for the $J' = \frac{3}{2} \leftarrow J'' = \frac{1}{2}$ M_J fits to Eq. (18) can be obtained from the parameter $(g_J'')_{eff}$ determined from the $J' = \frac{3}{2} \leftarrow J'' = \frac{1}{2}$ hyperfine structure fits using the relation

$$(g_J'')_{eff} = (g_J'') + \Delta g_J'', \tag{30}$$

where (g_J'') for $J'' = \frac{1}{2}$ is defined in Eqs. (11).

Analysis of the $J' = \frac{3}{2} \leftarrow J'' = \frac{1}{2}$ Hyperfine Structure

We begin the hyperfine analysis with the $J' = \frac{3}{2} \leftarrow J'' = \frac{1}{2}$ transitions, where patterns containing three components can be observed in which the sum of the intensities of the two weaker components is approximately equal to the intensity of the strongest component (see Fig. 4). Such patterns permit unambiguous quantum number assignments for the hyperfine structure to be established, since the basis set selection rule $\Delta M_I = 0$ requires the strongest component to be a transition involving a $J'' = \frac{1}{2}$ level with $M_F'' = \pm 1$, as described by Eq. (23), and the two weaker components to be transitions involving $J'' = \frac{1}{2}$ levels with $M_F'' = 0$, as described by the two roots in Eq. (27).

Table II presents all hyperfine measurements and assignments obtained for the $J' = \frac{3}{2} \leftarrow J'' = \frac{1}{2}$ transitions. The nine line measurements in each column are divided into groups of three, and are listed within each group in order of decreasing intensity. Blank entries indicate hyperfine components too weak to observe. Entries in parentheses indicate measurements with two assignments. When the $J'' = \frac{1}{2}$ level is described by Eq. (23), values for both M_I'' and M_J'' are given. When the $J'' = \frac{1}{2}$ level is described by Eq. (27), and is therefore a mixture of $M_I'' = -M_J'' = +\frac{1}{2}$ and $-\frac{1}{2}$ basis set functions, only a sign is given, indicating the sign to be used in Eq. (27).

In principle, each of the four $J' = \frac{3}{2} \leftarrow J'' = \frac{1}{2}$ molecular transitions (e.g., $F_{1e}(1) \leftarrow F_{2e}(1)$, $v = 0$) displays six high-field ($|M_J'| = \frac{1}{2}$) and three low-field ($|M_J'| = \frac{3}{2}$) hyperfine components in the spectrum recorded with any one of the three laser lines. The 27 lines from one molecular transition (or as many as were observed) were all treated together in a single least squares fit. One H_0 parameter was introduced and allowed to vary for each high-field or each low-field set of measurements included in the fit. In addition, the set of parameters h', k', $(g_J'')_{eff}$, f'', h'', and k'' was introduced and allowed to vary. Values for these parameters from the four fits, followed by one standard deviation in parentheses, are given in Table VI. Observed-minus-calculated magnetic field values from the fits are given in Table II.

Assignment of the spectra to $v = 0$ and $v = 1$ vibrational levels is consistent with the expectation that $v = 0$ transitions will be much stronger than $v = 1$ transitions, and that molecular parameters from analogous $v = 0$ and $v = 1$ spectra will be nearly identical. (Relative intensity estimates of about 0.06 for the ratio of corresponding $v = 1$ and $v = 0$ lines indicate a vibrational temperature somewhat above 1000°C.) It can be shown from the large change in B value with vibrational state (J), and from

TABLE VI

Parameters[a] from Least Squares Fits of the Hyperfine Structure

	$F_{1e}(1) - F_{2e}(1)$[b] v = 0		$F_{1e}(1) - F_{2e}(1)$[b] v = 1		$F_{1f}(1) - F_{2f}(1)$[b] v = 0		$F_{1f}(1) - F_{2f}(1)$[b] v = 1	
σ [G][c]	0.7		0.6		0.4		0.7	
h [MHz][d]	-11.06(43)	+13.26(45)	-11.70(33)	+14.99(33)	+0.78(20)	+71.56(16)	-1.96(43)	+68.63(29)
k [MHz/kG][d]	-0.13(8)	+0.19(8)	-0.15(29)	+0.13(29)	-0.18(2)	+0.10(3)	-0.23(3)	-0.01(5)
k_{calc}[e]	-0.12	+0.17	-0.12	+0.17	-0.17	+0.12	-0.17	+0.12
$(g_J'')_{eff}$[d]		-0.00430(5)		-0.00423(5)		+0.00087(5)		+0.00070(8)
$f'' \times 10^3$ [kG]$^{-2}$[d]		-0.0023(2)		-0.0013(3)		-0.0022(3)		-0.0015(4)

λ [μm]	M_J'	H_0 [kG]	$\partial E/\partial H$[f]	H_0 [kG]	$\partial E/\partial H$[f]	H_0 [kG]	$\partial E/\partial H$[f]	H_0 [kG]	$\partial E/\partial H$[f]
567.9	-1/2	15.8670(4)	-0.5189	13.0061(3)	-0.5274	8.3582(2)	-0.5624	6.0308(3)	-0.5672
567.9	-3/2	4.9275(4)	-1.8018	4.0932(4)	-1.7819	2.6865(2)	-1.8173	1.9577(4)	-1.7954
561.3	∓1/2[g]	4.4903(3)	-0.5809	1.7992(3)	-0.5882	2.2320(2)	+0.6193	4.4745(4)	+0.6235
561.3	∓3/2[g]	1.4683(5)	-1.8091	0.5968(4)	-1.7892	0.7516(2)	+1.8245	-	+1.8027
554.4	+1/2	6.4465(4)	+0.6393	9.0259(3)	+0.6456	12.5517(2)	+0.6737	14.7382(3)	+0.6773
554.4	+3/2	2.2070(4)	+1.8167	3.1221(3)	+1.7969	4.4031(2)	+1.8320	5.2135(4)	+1.8102

	$F_{1e}(3) - F_{1e}(2)$[h]		$F_{1f}(3) - F_{1f}(2)$[h]		$F_{1e}(2) - F_{1e}(1)$[i]		$F_{1f}(2) - F_{1f}(1)$[i]	
σ [G][c]	0.3		0.4		0.0		0.1	
h [MHz][d]	-8.89(19)	-10.23(20)	-3.51(7)	-3.20(9)	-10.227[j]	-9.93(2)	-3.201[j]	+1.06(3)
k [MHz/kG][d]	-0.25(5)	-0.07(4)	-0.71(3)	-0.48(3)	-0.07223[j]	+0.02(0)	-0.48332[j]	-0.38(1)
k_{calc}[e]	-0.42	-0.28	-0.65	-0.43		-0.12		-0.17

[a] Numbers in parentheses indicate one standard deviation of the last digit(s) given, as obtained from the least squares program.

[b] Data and Observed-minus-Calculated values in Table II. Fits carried out using Eq. (29).

[c] Standard deviation of the fit.

[d] Molecular constants appearing in Eqs. (23) or (27). Upper state constants on the left, lower state constants on the right.

[e] From Eq. (24) and the Frosch and Foley parameters in Table VII.

[f] The value of $(\partial E'/\partial H - \partial \bar{E}''/\partial H)$ in [MHz/G] at the center of the hyperfine structure characterized by the laser line, upper state quantum number M_J', and magnetic field indicated at the left. This value is obtained from the M_J fits and is not allowed to vary in the hyperfine fits.

[g] The - sign is to be used for the $F_{1e} - F_{2e}$ transitions, the + sign for the $F_{1f} - F_{2f}$ transitions.

[h] Data and Observed-minus-Calculated values for the simultaneously fit 118.6 μm and 118.8 μm hyperfine splittings for this transition are given in Table III. Fits were carried out using Eq. (28).

[i] Data and Observed-minus-Calculated values in Table III. Fits using Eq. (28).

[j] Fixed at the value obtained in the corresponding $F_1(3) - F_1(2)$ fit.

the 20 kG tuning range of our spectrometer, that only the $F_1(1) \leftarrow F_2(1)$ transition in Fig. 1 permits observation of $v = 1$ and $v = 0$ spectra with the same laser line.

Magnetic field positions for hypothetical transitions exhibiting no hyperfine interactions, which are required for the M_J fits of Section IV, can be calculated from the parameters in Table VI and an equation analogous to Eq. (29) with $h = k = \mu_n = 0$ for the upper and lower states.

$$H(M_J', M_J'') = H_0(M_J') - [(g_J'')_{eff} + f''H^2]\mu_B M_J'' H/[\partial E'/\partial H - \partial \bar{E}''/\partial H]. \quad (31)$$

Values for $H(M_J', M_J'')$ calculated from Eq. (31) are given in Table II.

Analysis of the Hyperfine Structure in Transitions with $J'' \geq \frac{3}{2}$

Hyperfine splittings in transitions with $J'' \geq \frac{3}{2}$ all correspond to the high field limit. Table VI thus contains hyperfine parameters obtained from these transitions by fitting the splittings in Table III to Eq. (28).

Signs for the splittings ΔH corresponding to the definition in Eq. (28) cannot be determined experimentally. Relative signs have been chosen in Table III so that one set of hyperfine parameters gives a good fit for all splittings within one rotational transition, and so that the signs of lower-state hyperfine constants determined from a $(J+1 \leftarrow J)$ transition match the signs of upper state constants determined from the corresponding $(J \leftarrow J-1)$ transition. Absolute signs for the hyperfine constants were unambiguously established from the fits of the $(\frac{3}{2} \leftarrow \frac{1}{2})$ transitions.

The larger number of hyperfine splittings available for the $(\frac{7}{2} \leftarrow \frac{5}{2})$ transitions permitted a least squares determination of the constants h and k in Eq. (28) for both the upper and lower state. The smaller number of hyperfine splittings for the $(\frac{5}{2} \leftarrow \frac{3}{2})$ transitions did not permit determination of all four of these constants, and least squares fits for these transitions were carried out with the $J = \frac{5}{2}$ constants set equal to values obtained in the $(\frac{7}{2} \leftarrow \frac{5}{2})$ fits.

Frosch and Foley Parameters

Table VII summarizes the values of the effective hyperfine coupling constant h determined from the various fits represented in Table VI. These eight values of h_{obs} correspond to zero-field quantities, and should be well described by the four Frosch and

TABLE VII

CH Hyperfine Parameters in [MHz]

State	J	h_{obs}[a]	h_{calc}[b]	Frosch and Foley Parameters[c]		
				this work[b,d]		Levy and Hinze[e]
$F_{2e}(1)$	1/2	+13.26	+13.34			
$F_{2f}(1)$	1/2	+71.56	+71.48	a	+52(2)	+(54 to 63)
$F_{1e}(1)$	3/2	-11.06, -9.93	-10.60	b	-74(3)	-(62 to 82)
$F_{1f}(1)$	3/2	+0.78, +1.08	+1.03	c	+52(7)	+(53 to 61)
$F_{1e}(2)$	5/2	-10.23	-10.45	d	+43.6(4)	+43.48
$F_{1f}(2)$	5/2	-3.20	-2.98			
$F_{1e}(3)$	7/2	-8.89	-8.97			
$F_{1f}(3)$	7/2	-3.51	-3.43			

[a] Values from Table VI. For use in Eq. (14a) in the absence of a magnetic field.

[b] From a least squares fit to Eqs. (13), with standard deviation σ = 0.4 MHz.

[c] Defined in reference (13).

[d] Numbers in parentheses represent one standard deviation of the last digit, as obtained from the least squares program.

[e] Reference (16): a, b and c from *ab initio* calculations; d from radioastronomy measurements.

Foley parameters a, b, c, and d (*13*) and Eqs. (13). Values for a, b, c, and d, as well as back-calculated values for h (i.e., h_{calc}), are also given in Table VII. It can be seen that the values of a, b, c, and d determined here agree well with values determined by Levy and Hinze (*16*) from a combination of radioastronomy measurement and ab initio calculation.

Once the parameters a, b, c, and d have been determined from fits of the values for the zero-field coupling constants h to Eqs. (13), it is possible to use Eqs. (22) and (24) to calculate values for the coefficient k of the magnetic field correction term in Eqs. (23) and (27). These calculated values for k are given in Table VI. They do not agree well with the observed values, which is probably the combined result of experimental uncertainties in the small hyperfine splittings and of the approximate theory used.

VI. DISCUSSION

The most interesting results of the present work are probably the rotational energy levels and Λ-doublings in Table V and the hyperfine parameters in Table VII.

The three well-determined rotational intervals in Table V are in good agreement with previous optical work (*2*). In principle, these three intervals could be combined with the optical measurements and used to improve the values of A, B, and D for CH. We prefer instead to wait for more extensive data on the three newly observed transitions shown in Fig. 1 (including observations with additional laser lines), since a thorough analysis of such data will provide five well-determined rotational intervals and an internal check.

Similar remarks can be made concerning refinement of the Λ-doubling parameters p and q. These exhibit a somewhat larger than expected dependence on the quantum number J (*2*), and more information, particularly for $F_2(N)$ levels, seems desirable before attempting to fit the data into some precise theoretical model. Analysis of the newly observed transitions will also permit a check on the Λ-doubling intervals in Table V, which were determined in the present work only by combining our values for interval *differences* with the radioastronomy value (*4*) for the $J = \frac{1}{2}$ interval.

The hyperfine parameters a, b, c, and d determined in the present work must be given significantly larger uncertainties than the values of one standard deviation shown in parentheses in Table VII. Our numbers thus do not represent an improvement over those of Levy and Hinze (*16*), but the good agreement between the two sets of parameters certainly represents an experimental confirmation of the theoretical results.

The Λ-doubling intervals in Table V may be of interest for astronomical searches for further microwave transitions in CH. We believe that three new Λ-doubling intervals are now determined with an uncertainty of about ±10 MHz. Future searches could thus be carried out at: (i) 0.710 GHz for the $F_1(1)$ state lying at a thermal excitation energy above the $J = \frac{1}{2}$ state equivalent to 26 K; (ii) at 4.857 GHz for the $F_1(2)$ state lying at an energy above $J = \frac{1}{2}$ equivalent to 105 K; or (iii) at 11.269 GHz for the $F_1(3)$ state at 227 K. Unfortunately, the present work does not yield an experimental determination of the 7 GHz splitting of the $F_2(2)$ state lying at an excitation energy above $J = \frac{1}{2}$ equivalent to 96 K.

ACKNOWLEDGMENTS

The authors are indebted to Dr. Carleton J. Howard for discussion and assistance throughout the course of this work, and to Drs. W. J. Lafferty, F. J. Lovas, and A. Weber for helpful criticism of the manuscript.

RECEIVED: August 2, 1977

REFERENCES

1. G. HERZBERG AND J. W. C. JOHNS, *Ap. J.* 158, 399–418 (1969).
2. A. E. DOUGLAS AND G. A. ELLIOTT, *Can. J. Phys.* 43, 496–502 (1965). (A. E. Douglas points out that the parity subscripts *c* and *d* in Table I of this reference must be interchanged.)
3. K. M. EVENSON, H. E. RADFORD, AND M. M. MORAN, JR., *Appl. Phys. Lett.* 18, 426–429 (1971).
4. O. E. H. RYDBECK, E. KOLLBERG, Å. HJALMARSON, A. SUME, J. ELLDÉR, AND W. M. IRVINE, *Ap. J. Suppl.* 31, 333–415 (1976).
5. J. O. HENNINGSEN, J. C. PETERSEN, F. R. PETERSEN, D. A. JENNINGS, AND K. M. EVENSON, in preparation.
6. F. R. PETERSEN, K. M. EVENSON, D. A. JENNINGS, J. S. WELLS, K. GOTO, AND J. J. JIMÉNEZ, *IEEE J. Quantum Electron.* QE-11, 838–843 (1975).
7. H. E. RADFORD, F. R. PETERSEN, D. A. JENNINGS, AND J. A. MUCHA, *IEEE J. Quantum Electron.* QE-13, 92–94 (1977).
8. S. F. DYUBKO, V. A. SVICH, AND L. D. FESENKO, *Zh. Tekh. Fiz.* 45, 2458–2461 (1975). English Translation: *Sov. Phys. Tech. Phys.* 20, 1536–1538 (1976).
9. G. HERZBERG, *Spectra of Diatomic Molecules*, Van Nostrand, Princeton, N.J., 1950.
10. J. M. BROWN, J. T. HOUGEN, K-P HUBER, J. W. C. JOHNS, I. KOPP, H. LEFEBVRE-BRION, A. J. MERER, D. A. RAMSAY, J. ROSTAS, AND R. N. ZARE, *J. Mol. Spectrosc.* 55, 500–503 (1975).
11. K. M. EVENSON, D. A. JENNINGS, F. R. PETERSEN, J. A. MUCHA, J. J. JIMÉNEZ, R. M. CHARLTON, AND C. J. HOWARD, *IEEE J. Quantum Electron.* QE-13, 442–444 (1977).
12. JON T. HOUGEN, "The Calculation of Rotational Energy Levels and Rotational Line Intensities in Diatomic Molecules," 49 pp., 1970, National Bureau of Standards (Washington, D.C. 20234) Monograph 115.
13. R. A. FROSCH AND H. M. FOLEY, *Phys. Rev.* 88, 1337–1349 (1952).
14. C. H. TOWNES AND A. L. SCHAWLOW, *Microwave Spectroscopy*, McGraw-Hill, New York, 1955.
15. R. S. MULLIKEN AND A. CHRISTY, *Phys. Rev.* 38, 87–119 (1931).
16. D. H. LEVY AND J. HINZE, *Ap. J.* 200, 236–238 (1975).